Supporting Information

Construction and cytotoxicity evaluation of peptide nanocarriers based on coiled-coil structures with a cyclic β-amino acid at the knob-into-hole interaction site

Monika Szefczyk, Natalia Szulc, Dominika Bystranowska, Anna Szczepańska, Juan Lizandra Pérez, Anita Dudek, Aleksandra Pawlak, Andrzej Ożyhar, Łukasz Berlicki*

* *monika.szefczyk@pwr.edu.pl*

Content **Page Number**

Table S1 Peptides analytical data.

Name	Sequence	Formula	Calculated M/z	Experimental M/z	Anal. HPLC t_r [min]
KSL	Ac-GEIAKSLKEIAKSLKWIAKSLKEIAKSLKG-NH_2	$C_{152}H_{266}N_{40}O_{41}$	[(M+2H)/2] 1655.5072 [(M+3H)/3] 1104.0074 [(M+4H)/4] 828.2576	[(M+2H)/2] 1655.9956 [(M+3H)/3] 1104.0122 [(M+4H)/4] 828.5255	12.273
KSX	Ac-GEIAKSXKEIAKSXKWIAKSXKEIAKSXKG-NH_2	$C_{152}H_{258}N_{40}O_{41}$	[(M+2H)/2] 1651.4760 [(M+3H)/3] 1101.3199 [(M+4H)/4] 826.2419	[(M+2H)/2] 1651.0057 [(M+3H)/3] 1101.3149 [(M+4H)/4] 826.2403	14.599
QAL	Ac-GEIAQALKEIAKALKEIAWALKEIAQALKG-NH_2	$C_{149}H_{253}N_{39}O_{41}$	[(M+3H)/3] 1082.9725 [(M+4H)/4] 812.4813 [(M+5H)/5] 650.1866	[(M+3H)/3] 1083.6342 [(M+4H)/4] 812.9787 [(M+5H)/5] 650.5803	15.711
QAX	Ac-GEIAQAXKEIAKAXKEIAWAXKEIAQAXKG-NH_2	$C_{149}H_{245}N_{39}O_{41}$	[(M+3H)/3] 1080.2849 [(M+4H)/4] 810.4657 [(M+5H)/5] 648.5741	[(M+3H)/3] 1080.2753 [(M+4H)/4] 810.7033 [(M+5H)/5] 648.5671	17.470
QGL	Ac-GEIAQGLKEIAKGLKEIAWGLKEIAQGLKG-NH_2	$C_{145}H_{245}N_{39}O_{41}$	[(M+2H)/2] 1595.9236 [(M+3H)/3] 1064.2849 [(M+4H)/4] 798.4657	[(M+2H)/2] 1595.8545 [(M+3H)/3] 1064.2573 [(M+4H)/4] 798.4626	13.040
QGX	Ac-GEIAQGXKEIAKGXKEIAWGXKEIAQGXKG-NH_2	$C_{145}H_{237}N_{39}O_{41}$	[(M+3H)/3] 1061.5974 [(M+4H)/4] 796.4500 [(M+5H)/5] 637.3616	[(M+3H)/3] 1061.5958 [(M+4H)/4] 796.4525 [(M+5H)/5] 637.3690	15.695

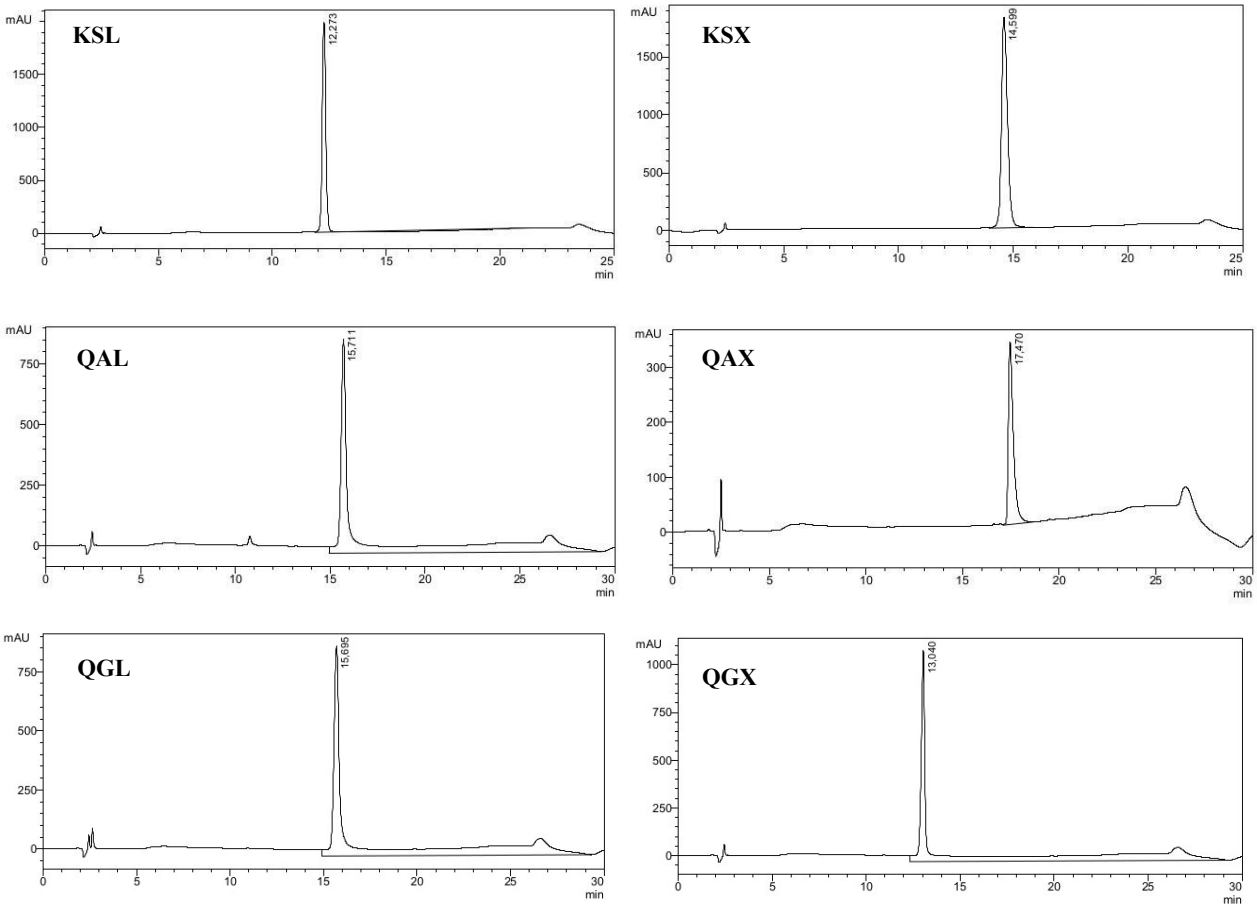

Figure S1. Analytical HPLC chromatograms of the studied peptides.

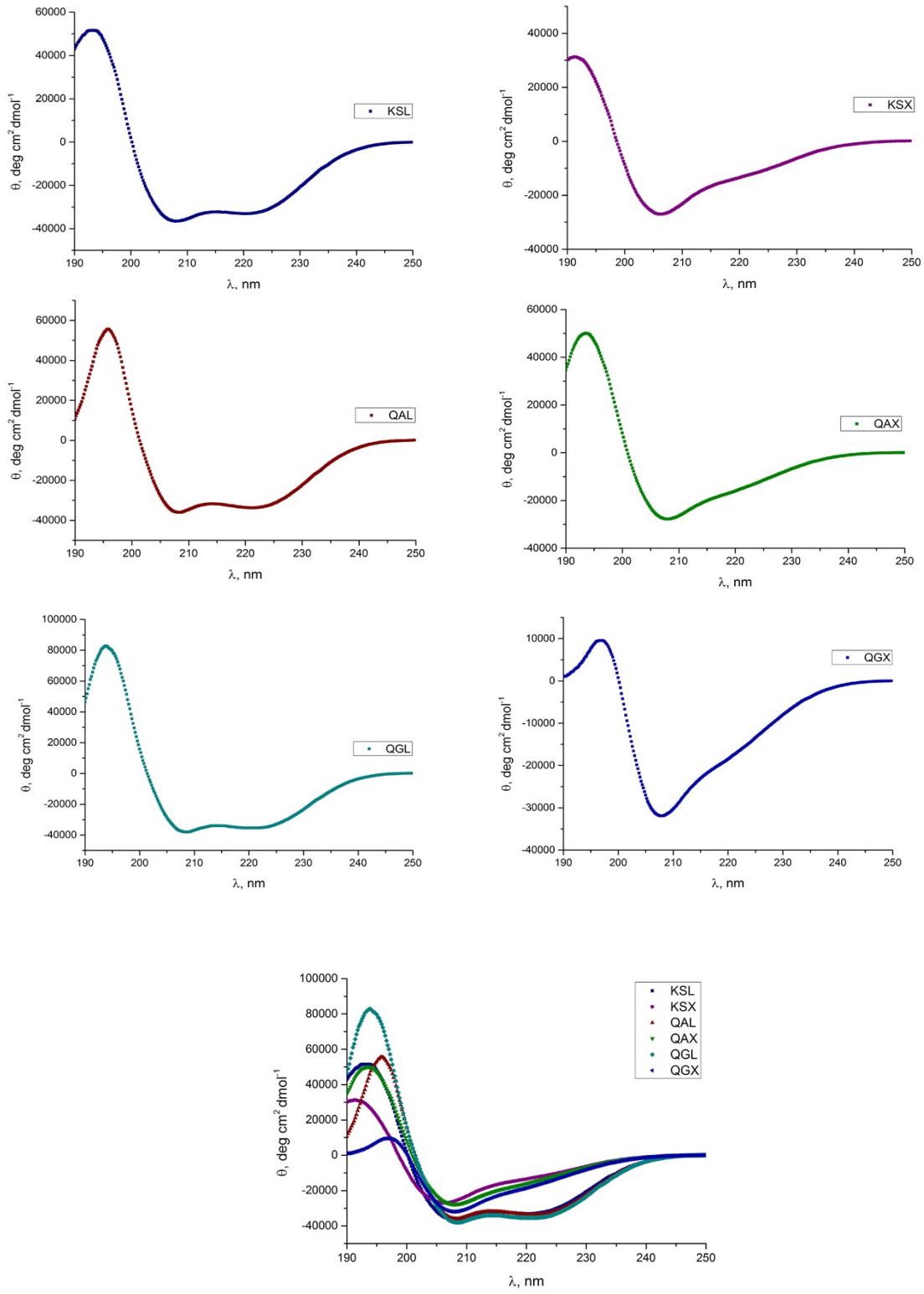

Figure S2. CD spectra of the studied peptides recorded in PB solution (0.05 M, pH = 7). C_{pep} = 150 μM.

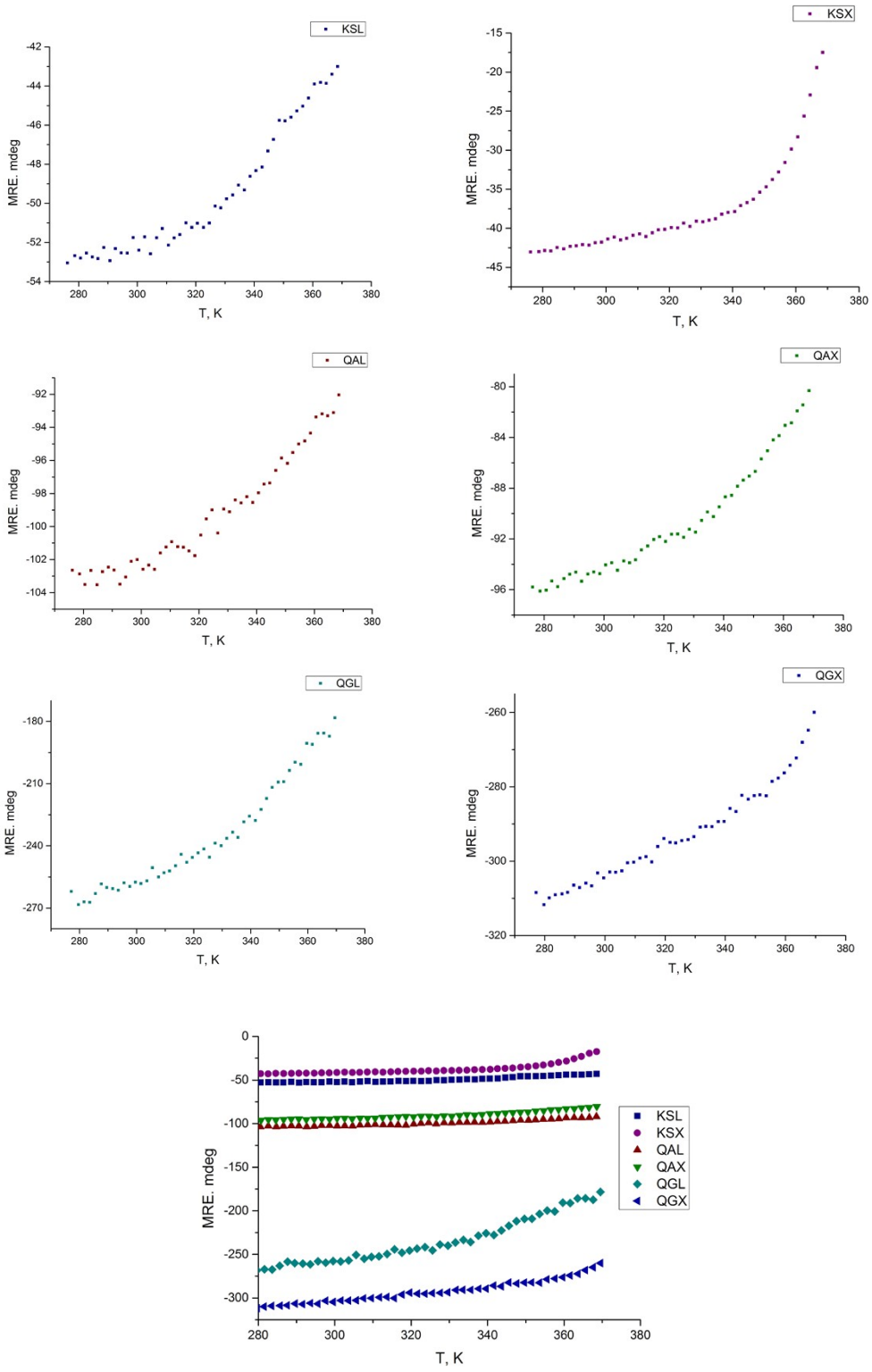

Figure S3. CD spectra for the thermal denaturation assay of the obtained peptides registered in PB solution (0.05 M, pH = 7). C_{pep} = 150 μM.

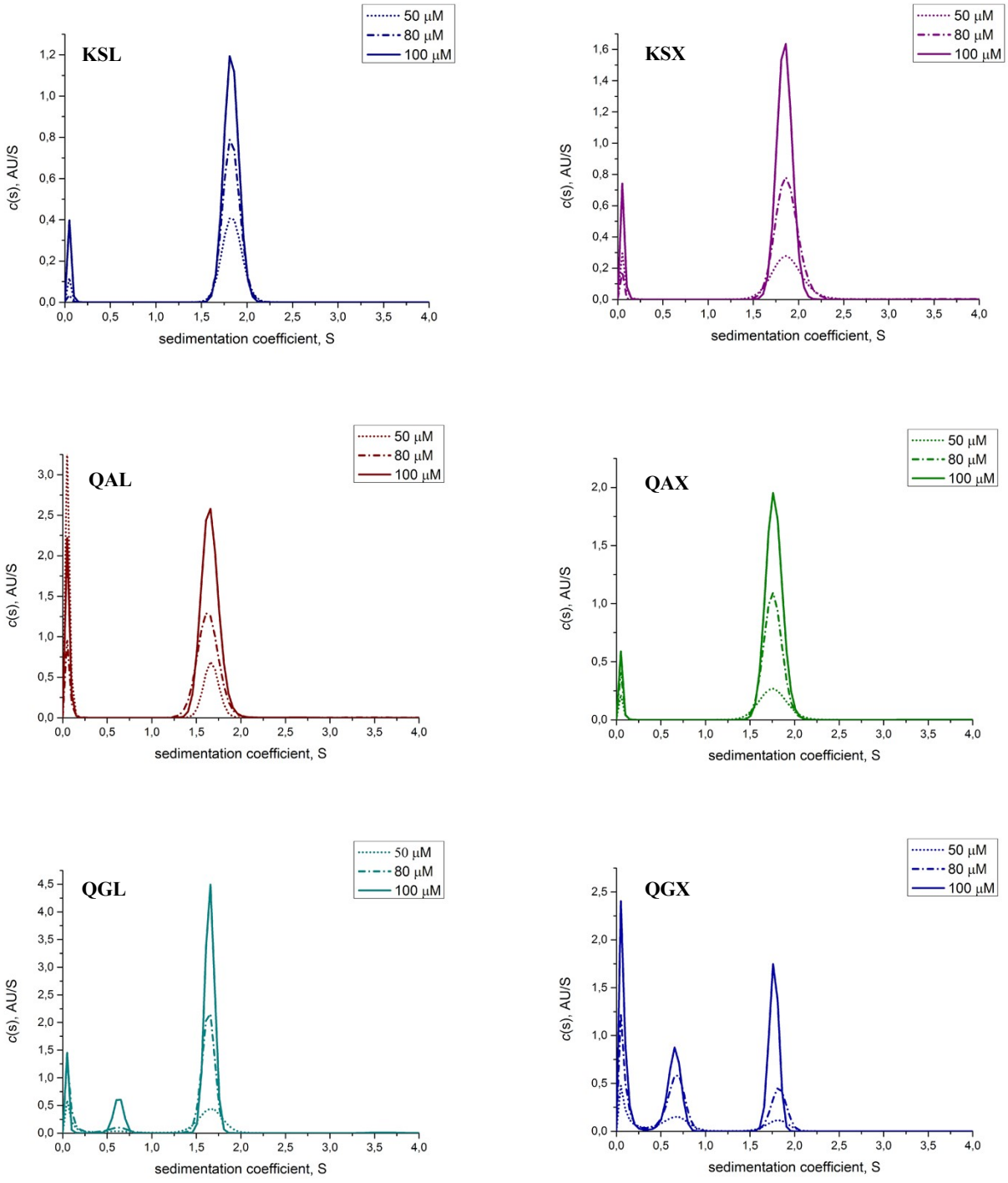

Figure S4. Sedimentation coefficient distributions *c*(s) obtained for different concentrations of the studied peptides resuspended in PB solution (0.05 M, pH = 7). Centrifugation was performed at 50 000 rpm and 20 °C.

Table S2. Results of SV-AUC experiments for the studies peptides.

Peptide	c (μM)	rmsd	$s_{20,w}$	f/f_0	MW_{app} (kDa)	Oligomerization state
KSL	50	0.007564	1.92	1.21	23.1	Heptamer (100%)
	80	0.007611	1.91	1.21	22.8	Heptamer (100%)
	100	0.007650	1.91	1.24	23.6	Heptamer (100%)
KSX	50	0.008804	1.96 3.54 8.37	1.21	23.2 56.5 204	Heptamer (83%) 17-mer (1%) 62-mer (16%)
	80	0.008627	1.96 3.95 7.17	1.20	22.5 64.6 158	Heptamer (88%) 20-mer (1%) 62-mer (11%)
	100	0.008761	1.93 4.62	1.21	22.6 83.8	Heptamer (99%) 25-mer (1%)
QAL	50	0.009425	1.74	1.22	19.4	Hexamer (100%)
	80	0.009048	1.70	1.24	19.2	Hexamer (100%)
	100	0.009842	1.73	1.23	19.4	Hexamer (100%)
QAX	50	0.009506	1.84	1.23	20.9	Hexamer (100%)
	80	0.009681	1.83	1.21	20.4	Hexamer (100%)
	100	0.010238	1.85	1.23	21.1	Hexamer (100%)
QGL	50	0.007862	0.679 1.72	1.27	4.788 19.3	Monomer\Dimer (9%) Hexamer (91%)
	80	0.008422	0.639 1.70	1.27	4.371 19.0	Monomer\Dimer (6%) Hexamer (94%)
	100	0.009317	0.653 1.72	1.27	4.513 19.3	Monomer\Dimer (13%) Hexamer (87%)
QGX	50	0.009055	0.680 1.873	1.20	4.35 19.9	Monomer\Dimer (65%) Hexamer (35%)
	80	0.009360	0.691 1.899	1.19	4.41 20.1	Monomer\Dimer (59%) Hexamer (41%)
	100	0.009773	0.676 1.843	1.18	4.20 18.9	Monomer\Dimer (40%) Hexamer (60%)

Numbers in brackets indicate the percentage of each fraction and are given considering 100% for the sum of the main indicated types of sedimenting species. rmsd – root-mean-square deviation; $s_{20,w}$ – sedimentation coefficient in the standard conditions (i.e. water, 20 °C); f/f_0 – frictional ratio (the ratio of the actual frictional coefficient to that for an anhydrous sphere with equal volume); MW_{app} – apparent molecular weight derived from SV-AUC experiments.

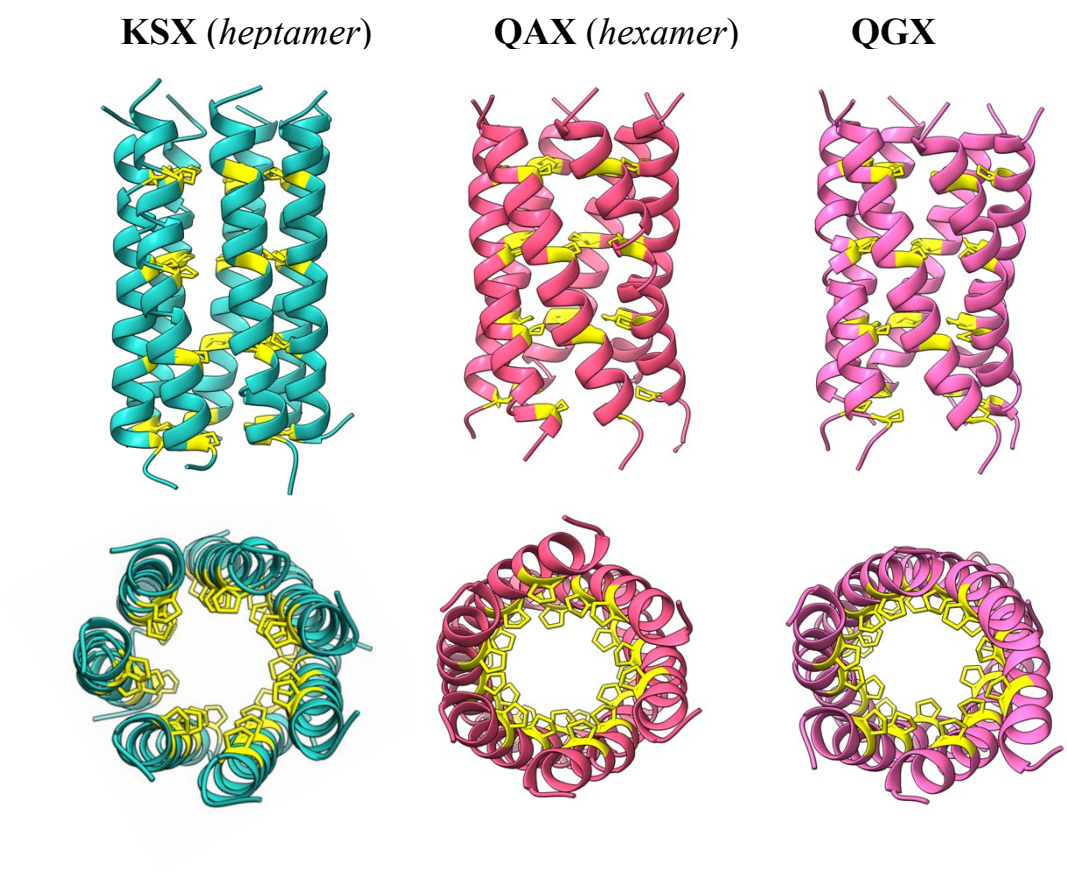

Figure S5. Theoretical models of α,β-peptides constructed to match the findings from the experiments. The helices were depicted using cartoon representation, with *trans*-ACPC highlighted in yellow.

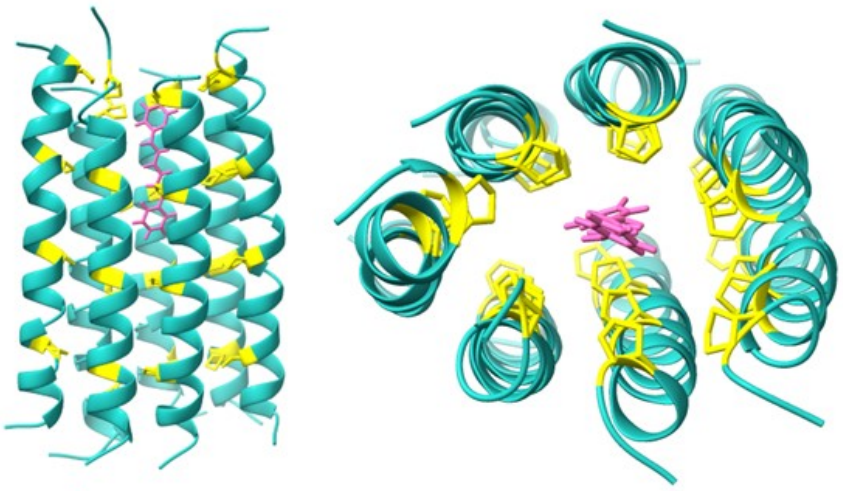

Figure S6. The distorted structure of **KSX** after MD with DPH. The ligand (pink) and the amino-acid residues making up the channel have been represented as sticks, with *trans*-ACPC highlighted in yellow.

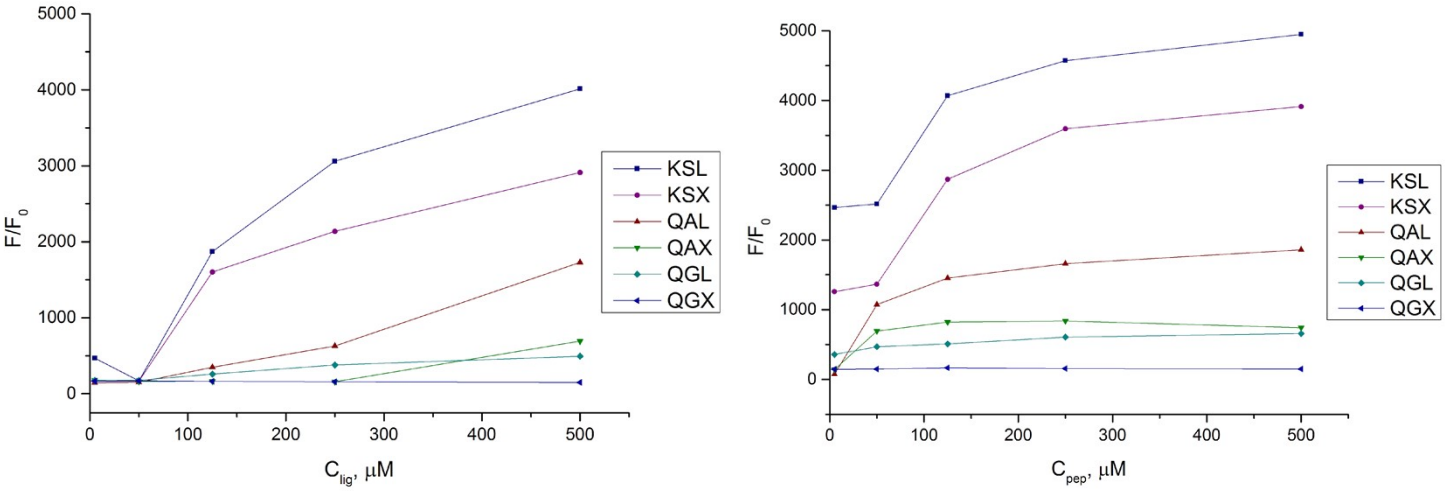

Figure S7. Ligand binding studies with DPH. The experiments were carried out in the concentration range of 5–500 μM. Either the 500 μM concentration of the peptide (left) or the ligand (right) was kept constant. The presented fluorescence values were obtained after 48 h of the experiment in PB (0.05 M, pH = 7), T = 25 ºC.

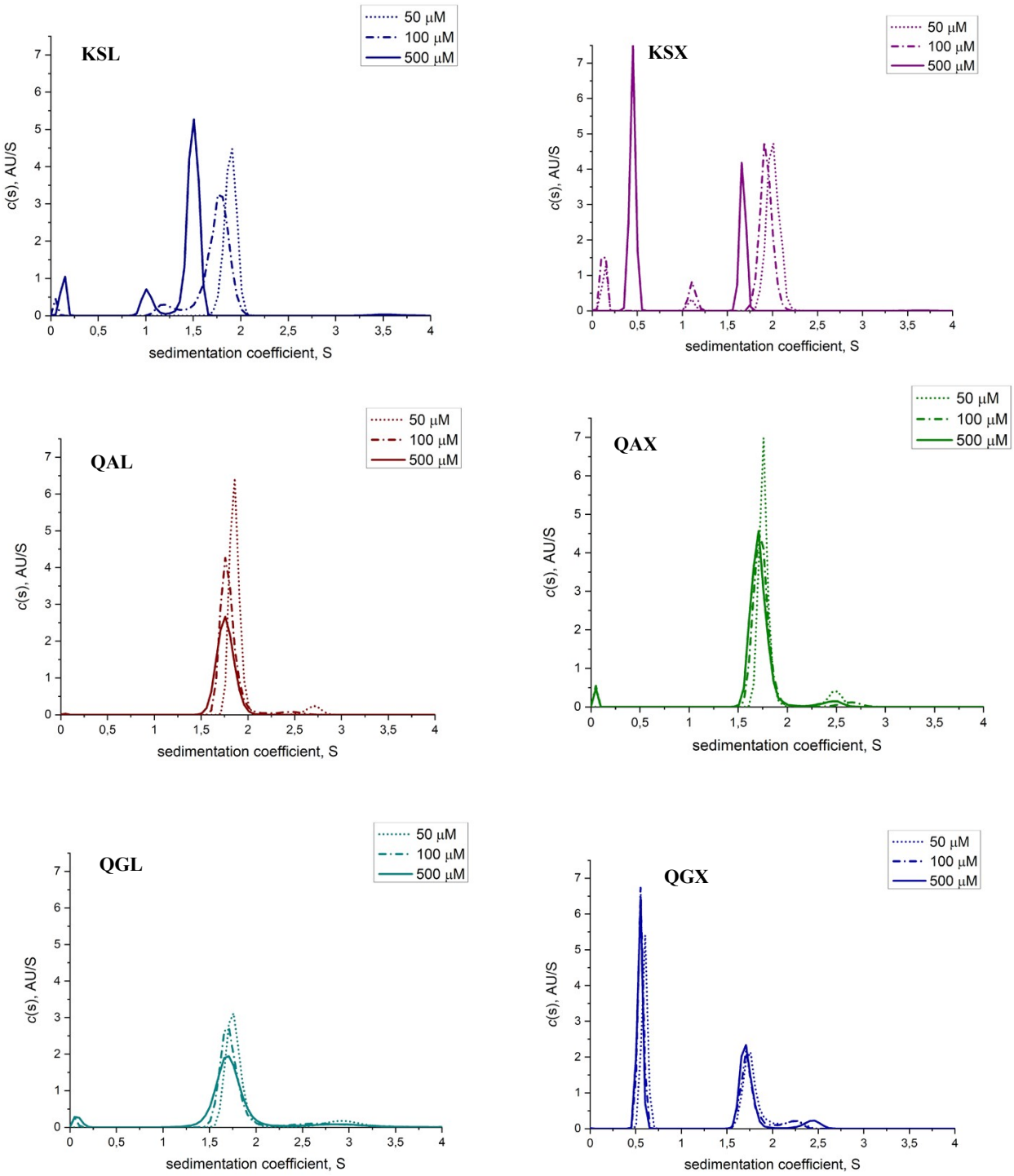

Figure S8. Sedimentation coefficient distributions *c*(s) obtained for the studied peptides (c = 50 μM) in the presence of the different DPH concentrations in PB (0.05 M, pH = 7). Centrifugation was performed at 50 000 rpm and 20 °C.

Table S3. Results of SV-AUC experiments for the studied peptides in the presence of different DPH concentrations.

Peptide	DPH c (μM)	rmsd	$s_{20,w}$	f/f_0	MW_{app} (kDa)	Oligomerization state
KSL (50 μM)	50	0.004810	1.98 8.31	1.12	21.5 185.2	Hexamer\Heptamer (82%) 56-mer (18%)
	100	0.004952	1.30 1.84	1.18	12.3 20.7	Tetramer (9%) Hexamer (91%)
	500	0.008302	1.07 1.56	1.39	11.8 20.8	Tetramer (11%) Hexamer (89%)
KSX (50 μM)	50	0.004959	1.15 2.10	1.16	9.75 24.0	Trimer (4%) Heptamer (96%)
	100	0.006913	1.16 2.02	1.21	10.6 24.1	Trimer (10%) Heptamer (90%)
	500	0.005598	0.47 1.75	1.31	3.05 21.9	Monomer (60%) Heptamer (40%)
QAL (50 μM)	50	0.006390	1.94 2.81	1.17	21.1 36.9	Hexamer (95%) 12-mer (5%)
	100	0.007231	1.87 2.55	1.19	20.6 32.8	Hexamer (97%) 10-mer (3%)
	500	0.009743	1.84	1.15	19.1	Hexamer (100%)
QAX (50 μM)	50	0.007358	1.84 2.59	1.30	22.8 38.1	Hexamer\Heptamer (91%) 12-mer (9%)
	100	0.006354	1.81 2.74	1.27	21.4 40.0	Hexamer (96%) 12-mer\13-mer (4%)
	500	0.006478	1.79 2.54	1.28	21.3 36.3	Hexamer (96%) 11-mer\12-mer (4%)
QGL (50 μM)	50	0.006046	1.84 3.07	1.20	19.3 41.9	Hexamer (87%) 13-mer (13%)
	100	0.005336	1.79 2.95	1.23	19.5 41.1	Hexamer (88%) 13-mer (12%)
	500	0.005283	1.78 3.05 4.94	1.24	19.5 43.5 89.6	Hexamer (90%) 13-mer (9%) 28-mer (1%)
QGX	50	0.009115	0.62	1.37	4.63	Monomer\Dimer (49%)

(50 μM)			1.85		23.8	Heptamer\Octamer (45%)
			2.35		34.0	10-mer (6%)
	100	0.008530	0.58	1.43	4.43	Monomer\Dimer (56%)
			1.81		24.6	Heptamer\Octamer (39%)
			2.32		35.6	10-mer (5%)
	500	0.007947	0.57	1.44	4.38	Monomer\Dimer (52%)
			1.79		24.4	Heptamer\Octamer (42%)
			2.52		40.8	12-mer\13-mer (6%)

Numbers in brackets indicate the percentage of each fraction and are given considering 100% for the sum of the main indicated types of sedimenting species. rmsd – root-mean-square deviation; $s_{20,w}$ – sedimentation coefficient in the standard conditions (i.e. water, 20 °C); f/f_0 – frictional ratio (the ratio of the actual frictional coefficient to that for an anhydrous sphere with equal volume); MW_{app} – apparent molecular weight derived from SV-AUC experiments.

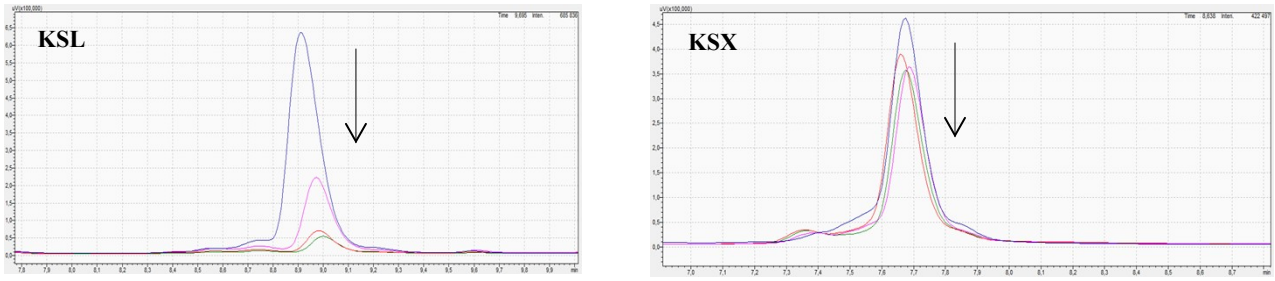

Figure S9. HPLC chromatograms obtained from proteolytic studies conducted on KSL and KSX in the presence of chymotrypsin (1:100 w/w) in 100 mM Tris-HCl buffer (pH = 8.0). Measurements were taken every 24 hours.

Table S4. The results obtained from proteolytic studies conducted on KSL and KSX in the presence of chymotrypsin (1:100 w/w) in 100 mM Tris-HCl buffer (pH = 8.0).

	Time [days]	**Area**	**% Degradation**
KSL	0	6630376	0
	1	2120975	68.0
	2	772730	88.3
	3	460968	93.0
KSX	0	5542357	0
	1	4438033	19.9
	2	4209830	24.0
	3	4092707	26.2

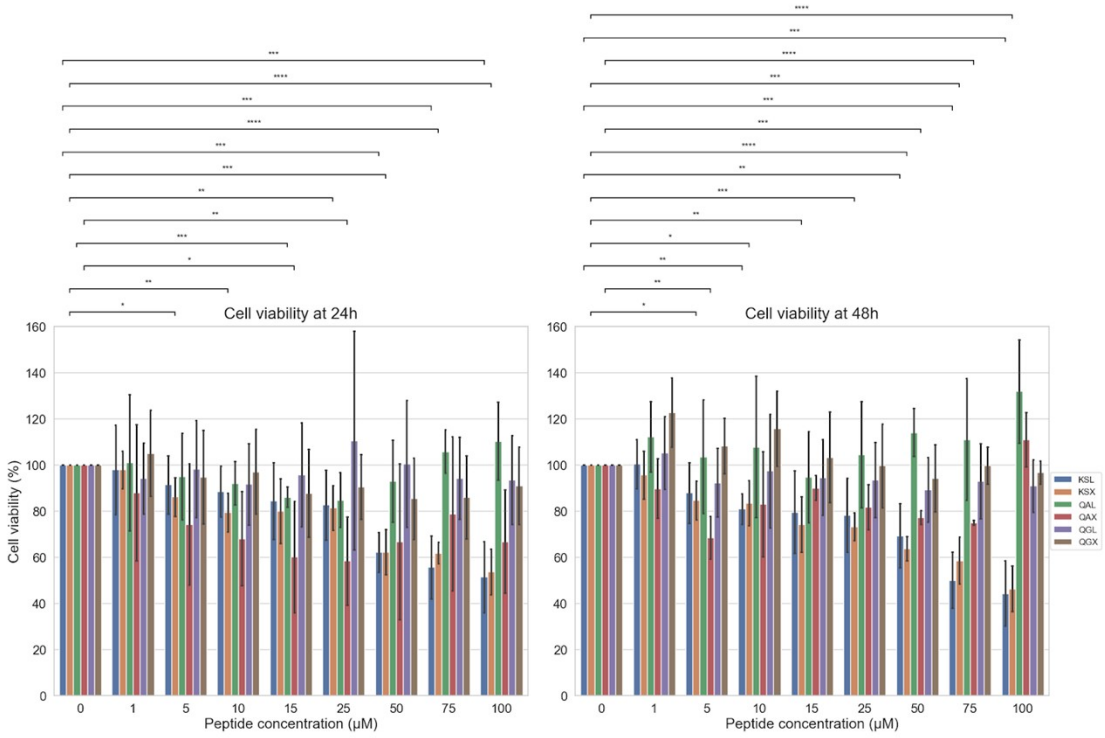

Figure S10. Cell viability of 3T3-NIH fibroblast cells treated with different peptide nanocarriers at varying concentrations (1-100 μM) after 24 and 48 hours of incubation, as assessed using the MTT assay. Results are expressed as the percentage of viable cells relative to untreated controls. Bars represent mean ± standard deviation (n ≤ 4). Statistical significance between groups was determined using three-way ANOVA followed by Tukey's HSD post hoc test, with significant differences indicated by asterisks (* $p \leq 0.05$, ** $p \leq 0.01$, *** $p \leq 0.001$, **** $p \leq 0.0001$). Peptides include KSL, KSX, QAL, QAX, QGL, and QGX.

Table S5. Summary of the results obtained for docking of DPH ligand to the initial models.

Receptor	**Number of helices**	**Best binding mode [kcal/mol]**	
		Structure without *trans*-ACPC	**Structure with *trans*-ACPC**
QAL	7	-8.4	-8.2
QGL	9	-6.3	-7.4

KSL	6	-8.9	-7.3

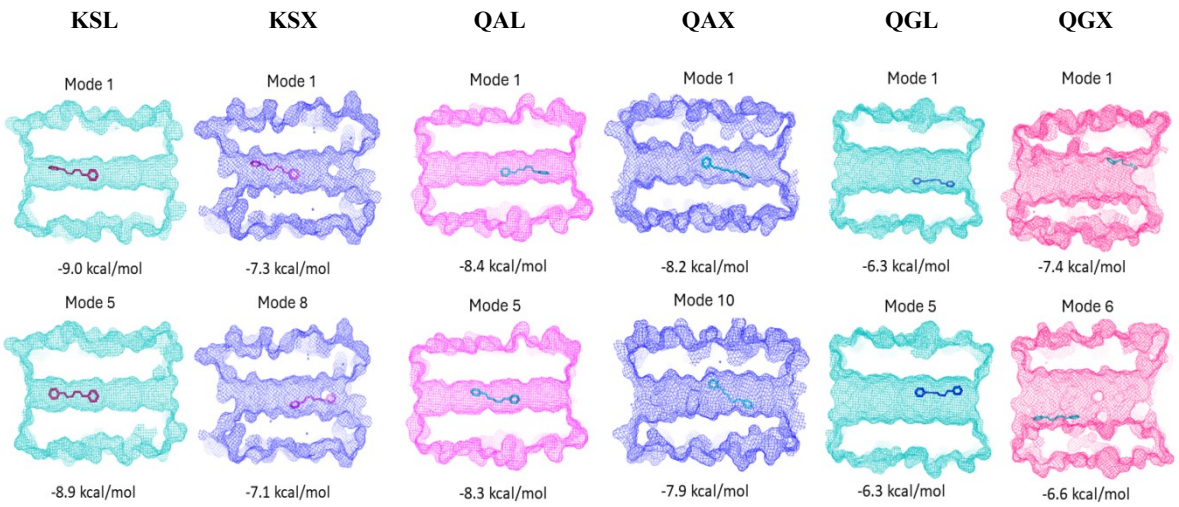

Figure S11. The results of docking for **KSL**, **KSX**, **QAL**, **QAX**, **QGL**, and **QGX**, respectively. For each, two representative binding modes of DPH have been displayed.

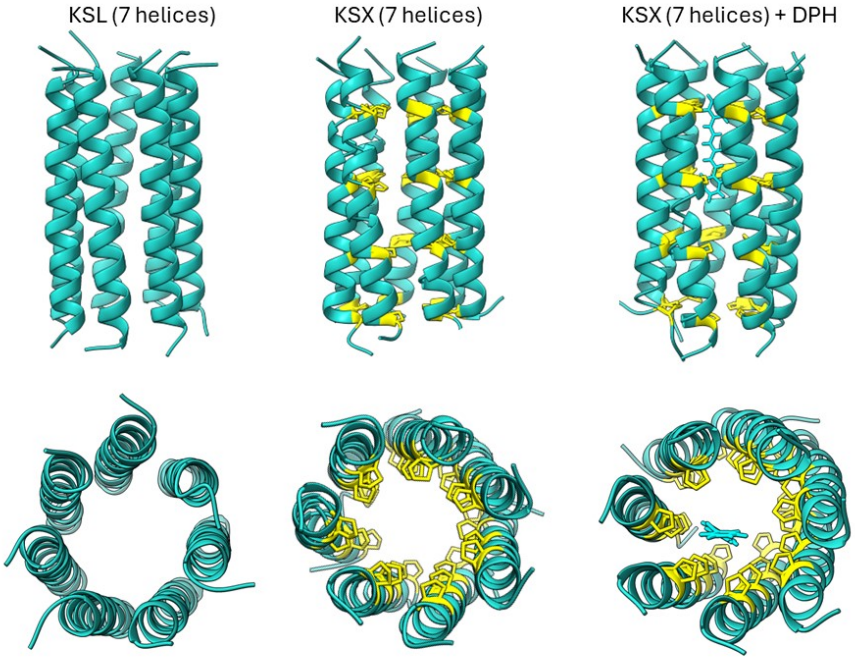

Figure S12. The updated structures of **KSL** and **KSX** with 7 helices. In the last step, DPH was docked in the channel (right).

Table S6. Summary of the results obtained for docking of two DPH ligands to **KSL**.

Receptor	Number of helices	Number of DPH molecules	Best binding mode [kcal/mol]	
			Structure without *trans*-ACPC	Structure with *trans*-ACPC
KSL	7	1	-8.0	-7.6
		2	-10.6	-10.3

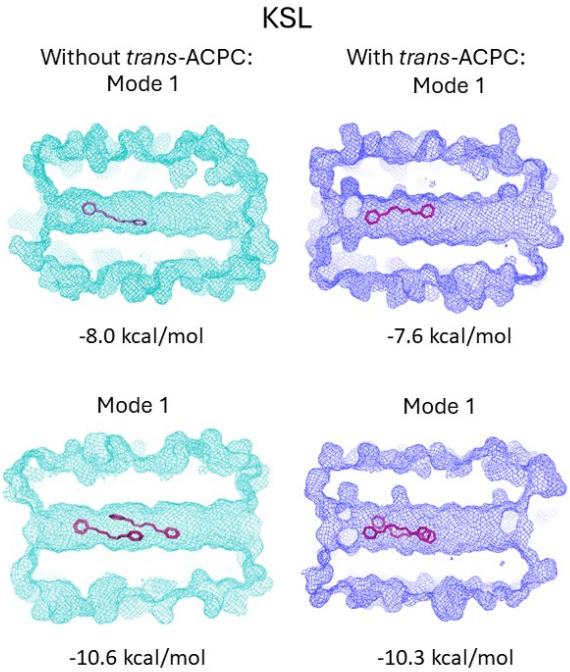

Figure S13. The results of docking for the updated models of **KSL** and **KSX**.

ANALYSIS OF MOLECULAR DYNAMICS

Table Sa. Summary of MD results. RoG – Radius of gyration; Distances 1, 2 – distances between two atoms on the periphery of the channel, specified separately for each peptide.

	QAX		QGX		KSX			KSL		
	with DPH	No DPH	with DPH	No DPH	With DPH	No DPH	2 DPH	With DPH	No DPH	2 DPH
RoG [Å]	16.36 ± 0.076	16.447 ± 0.093	16.058 ± 0.056	16.088 ± 0.063	17.14 ± 0.066	17.039 ± 0.052	17.088 ± 0.073	17.05 ± 0.04	17.14 ± 0.046	17.12 ± 0.046
RMSD Cα [Å]	1.743 ± 0.269	1.463 ± 0.2153	1.209 ± 0.118	1.449 ± 0.148	2.115 ± 0.393	2.332 ± 0.318	2.556 ± 0.591	1.046 ± 0,106	1.311 ± 0.187	1.340 ± 0.156
Distance 1 [Å]	9.646± 0.901	9.41 ± 0.599	10.677 ± 1.18	10.768 ± 1.206	12.08 ± 1.277	11.381 ± 0.965	8.403 ± 2.331	9.399 ± 1.21	10.736 ± 0.893	10.511 ± 0.884
Distance 2 [Å]	9.433 ± 0.827	9.55 ± 0.826	10.795 ± 0.987	10.846 ± 1.028	11.91 ± 1.555	11.530 ± 1.168	12.616 ± 1.489	10.512 ± 1.14	11.259 ± 1.273	11.269 ± 1.223
helix	6		6		7			7		

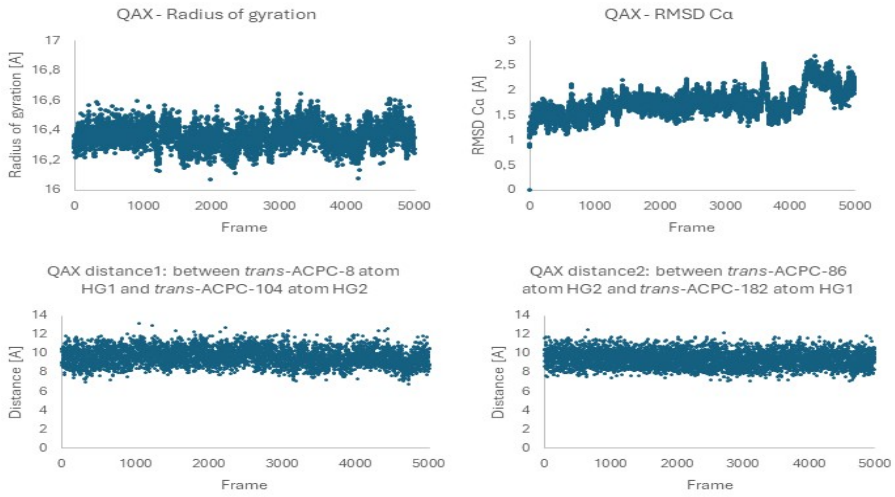

Figure Sb. The changes in the structure of **QAX** with **docked DPH** over the course of a 500-ns molecular dynamics simulation. This includes variations in the radius of gyration, RMSD of the alpha carbon atom, as well as measurements of distance 1 (between a hydrogen atom of *trans*-ACPC residues 8 and 104) and distance 2 (between *trans*-ACPC residues 86 and 182). The selection of atoms for distance 1 and distance 2 serves as a means to monitor the dimensions of the channel at both ends.

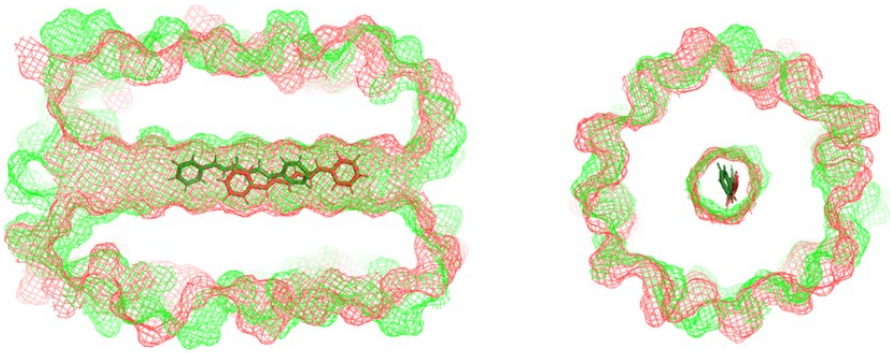

Figure Sc. The starting structure of **QAX** (red) with **docked DPH** molecule superimposed on the 500 ns structure (green) for comparison.

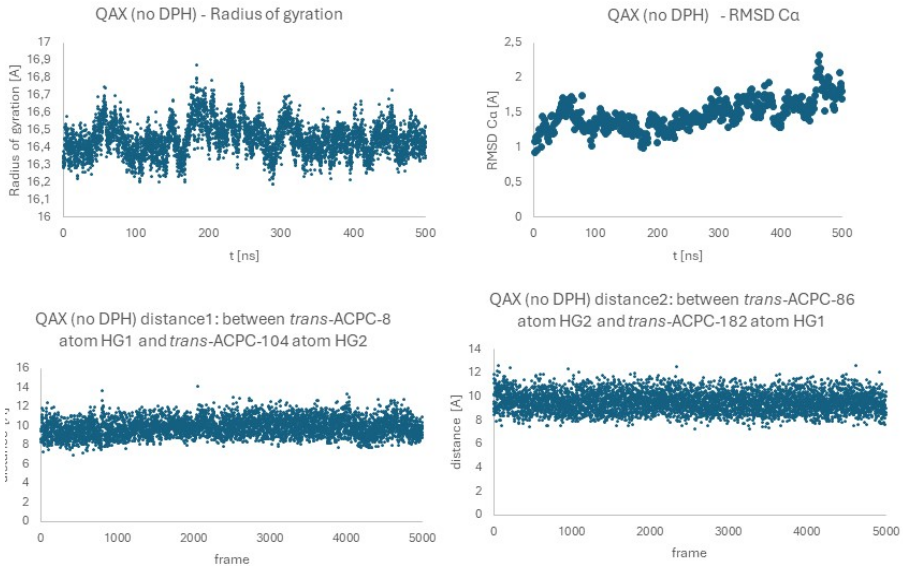

Figure Sd. The changes in the structure of **QAX without the ligand** over the course of a 500-ns molecular dynamics simulation. This includes variations in the radius of gyration, RMSD of the alpha carbon atom, as well as measurements of distance 1 (between a hydrogen atom of *trans*-ACPC residues 8 and 104) and distance 2 (between *trans*-ACPC residues 86 and 182). The selection of atoms for distance 1 and distance 2 serves as a means to monitor the dimensions of the channel at both ends.

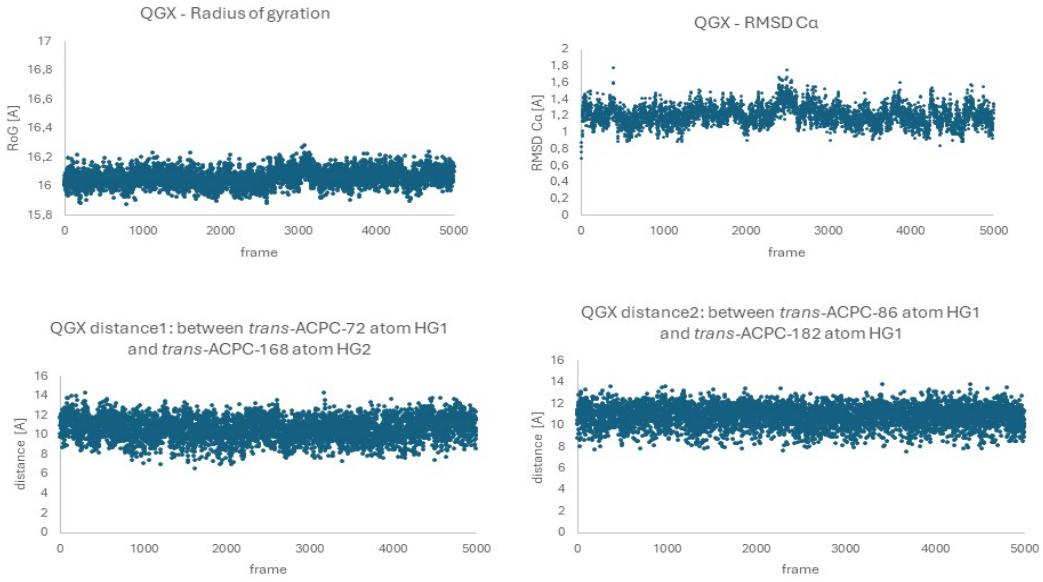

Figure Se. The changes in the structure **QGX** with **docked DPH** over the course of a 500-ns molecular dynamics simulation. This includes variations in the radius of gyration, RMSD of the alpha carbon atom, as well as measurements of distance 1 (between a hydrogen atom of *trans*-ACPC residues 72 and 168) and distance 2 (between *trans*-ACPC residues 86 and 182). The selection of atoms for distance 1 and distance 2 serves as a means to monitor the dimensions of the channel at both ends.

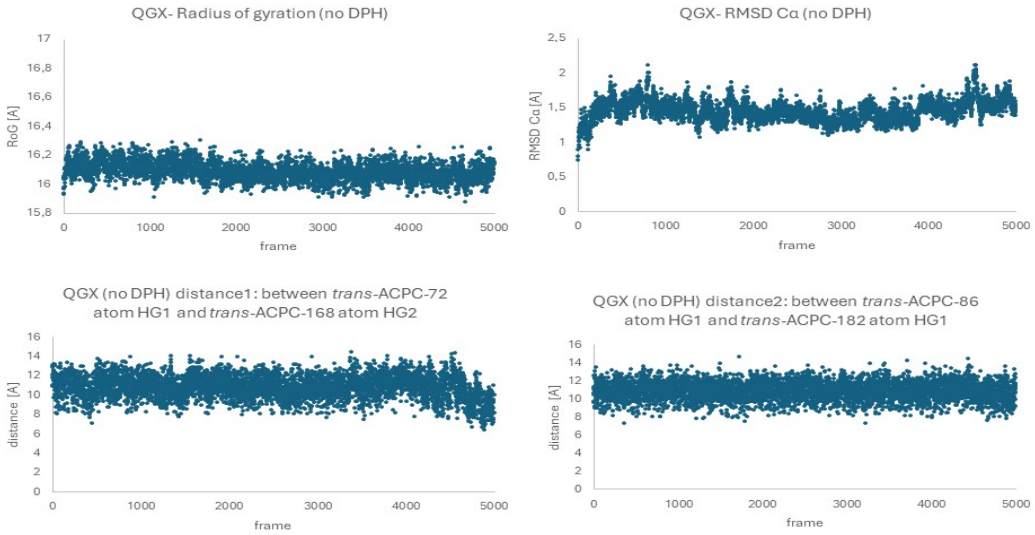

Figure Sf. The changes in the structure of **QGX without the ligand** over the course of a 500-ns molecular dynamics simulation. This includes variations in the radius of gyration, RMSD of the alpha carbon atom, as well as measurements of distance 1 (between a hydrogen atom of *trans*-ACPC residues 72 and 168) and

distance 2 (between *trans*-ACPC residues 86 and 182). The selection of atoms for distance 1 and distance 2 serves as a means to monitor the dimensions of the channel at both ends.

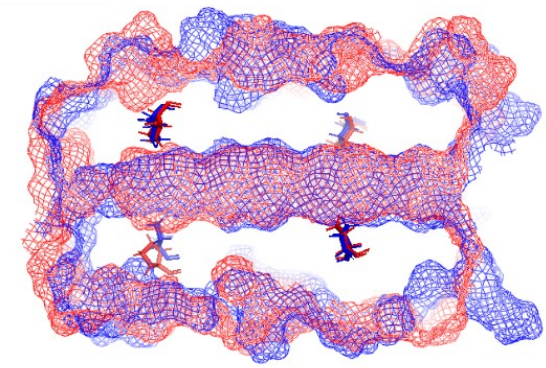

Figure Sg. The **400-ns** (frame 4000) structure of **QGX** (red) superimposed on the **500-ns** structure (navy) for comparison. *Trans*-ACPC residues 72, 168, 86 and 182 have been depicted in stick representation to show their displacement.

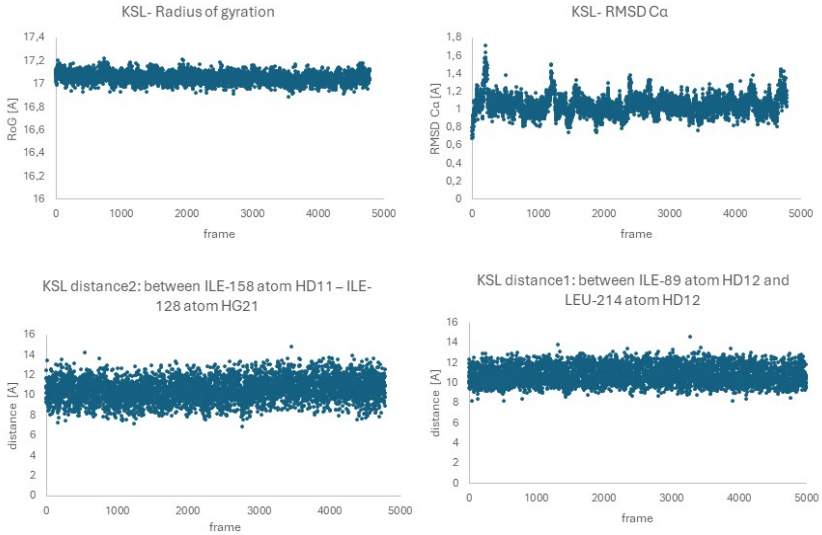

Figure Sh. The changes in the structure of **KSL** with **docked DPH** over the course of a 500-ns molecular dynamics simulation. This includes variations in the radius of gyration, RMSD of the alpha carbon atom, as

well as measurements of distance 1 (between a hydrogen atom of isoleucine residues 158 and 128) and distance 2 (between isoleucine residues 89 and 214). The selection of atoms for distance 1 and distance 2 serves as a means to monitor the dimensions of the channel at both ends.

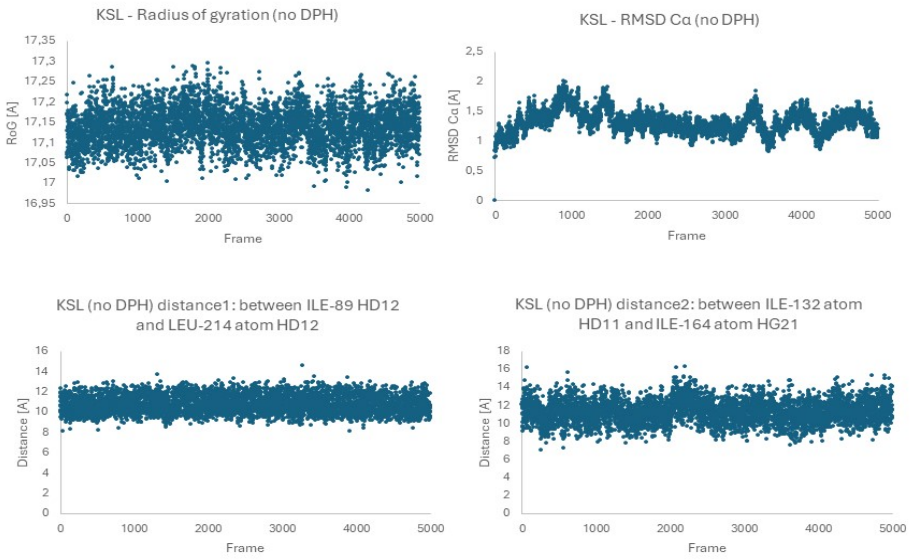

Figure Si. The changes in the structure of **KSL** without the ligand over the course of a 500-ns molecular dynamics simulation. This includes variations in the radius of gyration, RMSD of the alpha carbon atom, as well as measurements of distance 1 (between a hydrogen atom of isoleucine residues 158 and 128) and distance 2 (between isoleucine residues 89 and 214). The selection of atoms for distance 1 and distance 2 serves as a means to monitor the dimensions of the channel at both ends.

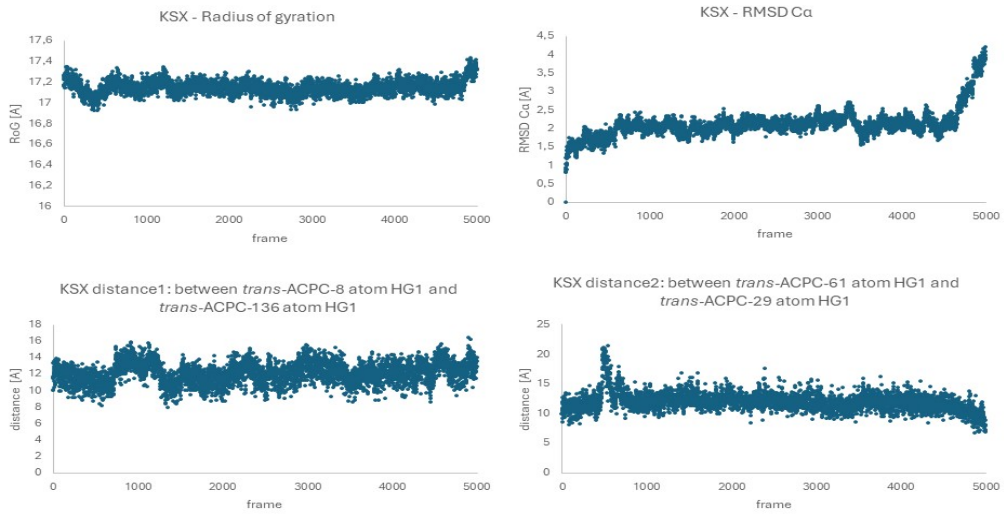

Figure Sj. The changes in the structure of **KSX** with **docked DPH** over the course of a 500-ns molecular dynamics simulation. This includes variations in the radius of gyration, RMSD of the alpha carbon atom, as well as measurements of distance 1 (between a hydrogen atom of *trans*-ACPC residues 8 and 136) and distance 2 (between *trans*-ACPC residues 61 and 29). The selection of atoms for distance 1 and distance 2 serves as a means to monitor the dimensions of the channel at both ends.

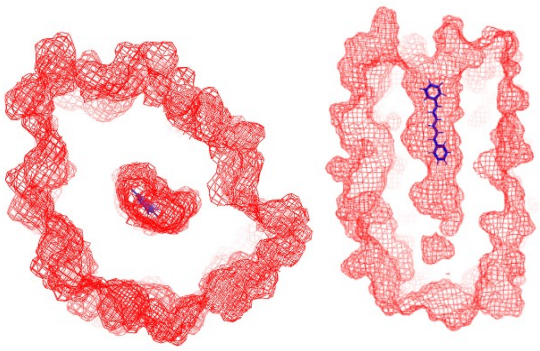

Figure Sk. Mesh representation of **KSX** after 500-ns of Molecular Dynamics, shown from the top (left) and side (right). The DPH molecule has been drawn using sticks. Around 470 ns the tunnel starts to close around the ligand.

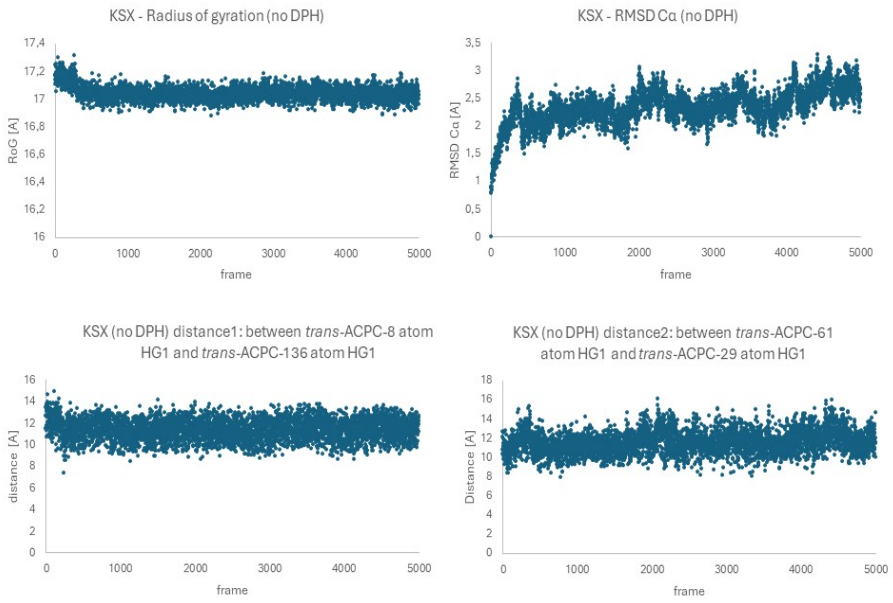

Figure Sl. The changes in the structure of **KSX** without the ligand over the course of a 500-ns molecular dynamics simulation. This includes variations in the radius of gyration, RMSD of the alpha carbon atom, as well as measurements of distance 1 (between a hydrogen atom of *trans*-ACPC residues 8 and 136) and distance 2 (between *trans*-ACPC residues 61 and 29). The selection of atoms for distance 1 and distance 2 serves as a means to monitor the dimensions of the channel at both ends.

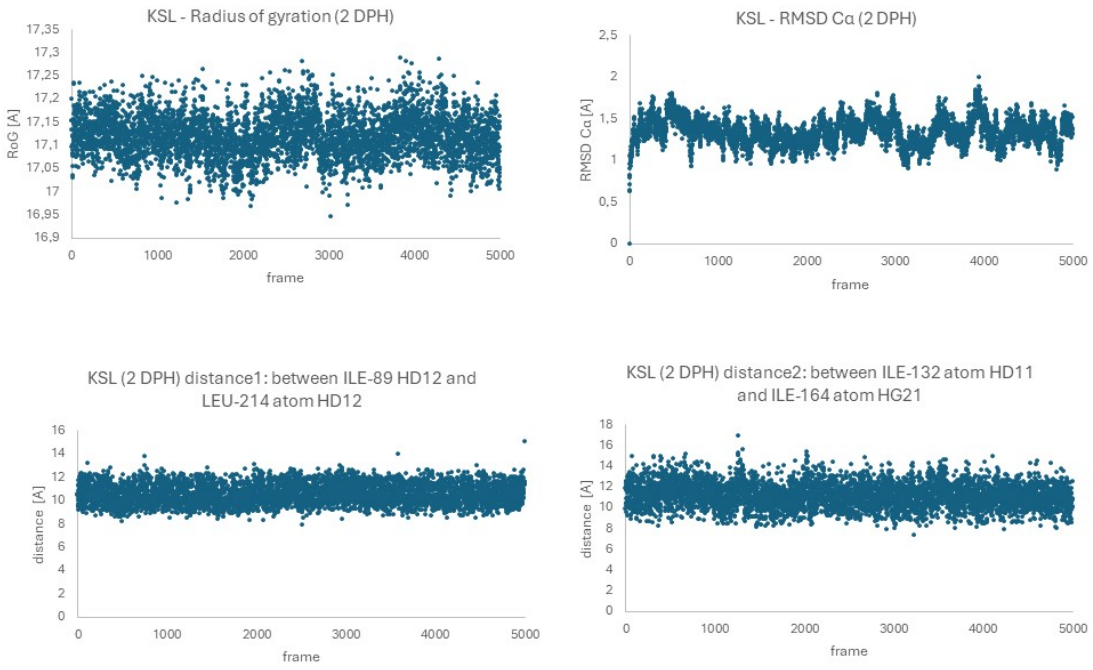

Figure Sm. The changes in the structure of **KSL** with two DPH ligands over the course of a 500-ns molecular dynamics simulation. This includes variations in the radius of gyration, RMSD of the alpha carbon atom, as well as measurements of distance 1 (between a hydrogen atom of Ile residue 89 and Leu 214) and distance 2 (between Ile residues 132 and 164). The selection of atoms for distance 1 and distance 2 serves as a means to monitor the dimensions of the channel at both ends.

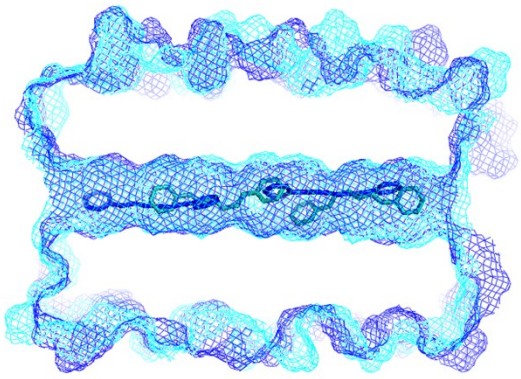

Figure Sn. The starting structure of **KSL** (cyan) with **two docked DPH** molecules superimposed on the 500 ns structure (navy) for comparison.

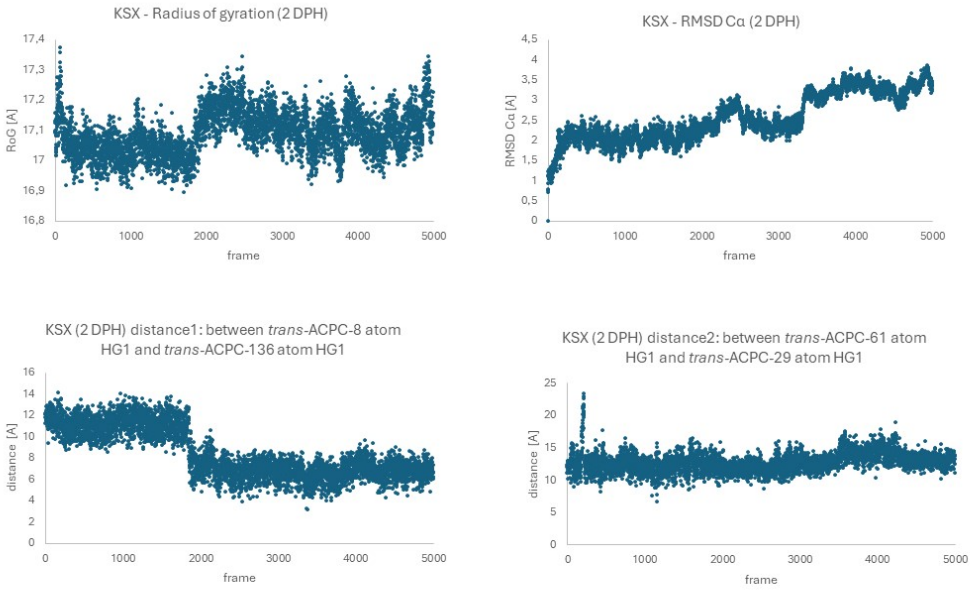

Figure So. The changes in the structure of **KSX** with two DPH ligands over the course of a 500-ns molecular dynamics simulation. This includes variations in the radius of gyration, RMSD of the alpha carbon atom, as well as measurements of distance 1 (between a hydrogen atom of *trans*-ACPC residues 8 and 136) and distance 2 (between *trans*-ACPC residues 61 and 29). The selection of atoms for distance 1 and distance 2 serves as a means to monitor the dimensions of the channel at both ends.

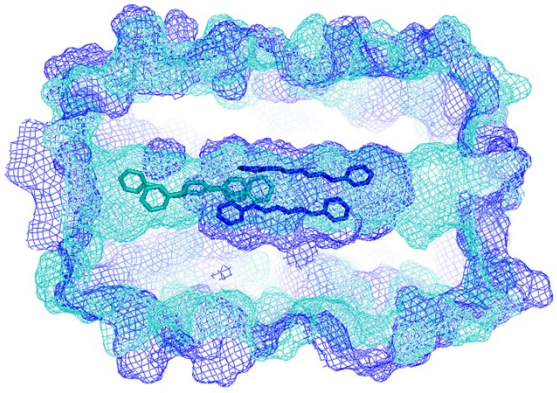

Figure Sp. The starting structure of **KSX** (cyan) with **two docked DPH** molecules superimposed on the 500 ns structure (navy) for comparison. Around 200 ns the tunnel starts to close around the ligands, which moved towards the center of the barrel.

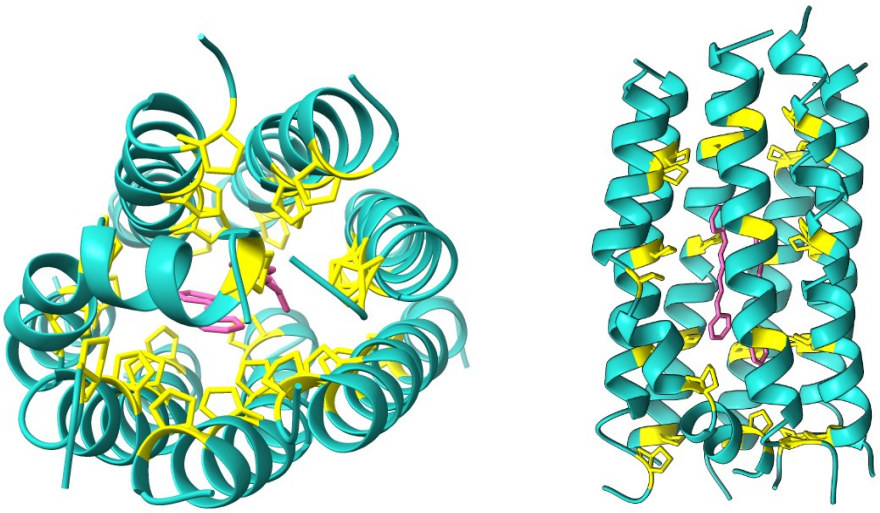

Figure Sr. Cartoon representation of **KSX** with two ligand molecules after 500-ns of Molecular Dynamics, shown from the top (left) and side (right). The DPH molecules (pink) and *trans*-ACPC residues (yellow) have been drawn using sticks. Around 200 ns the tunnel starts to close, and a helix contorts to cover one of its' openings.

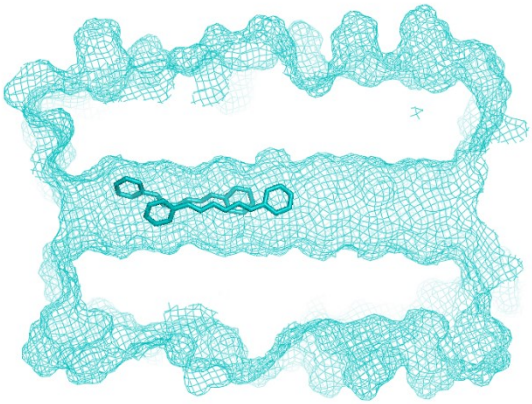

Figure Ss. The result of a 24-ns Molecular Dynamics simulation of an alternative docking position of two DPH ligands to **KSX**. The obtained structure resembles the starting point for calculations depicted on **Figure Sp.**

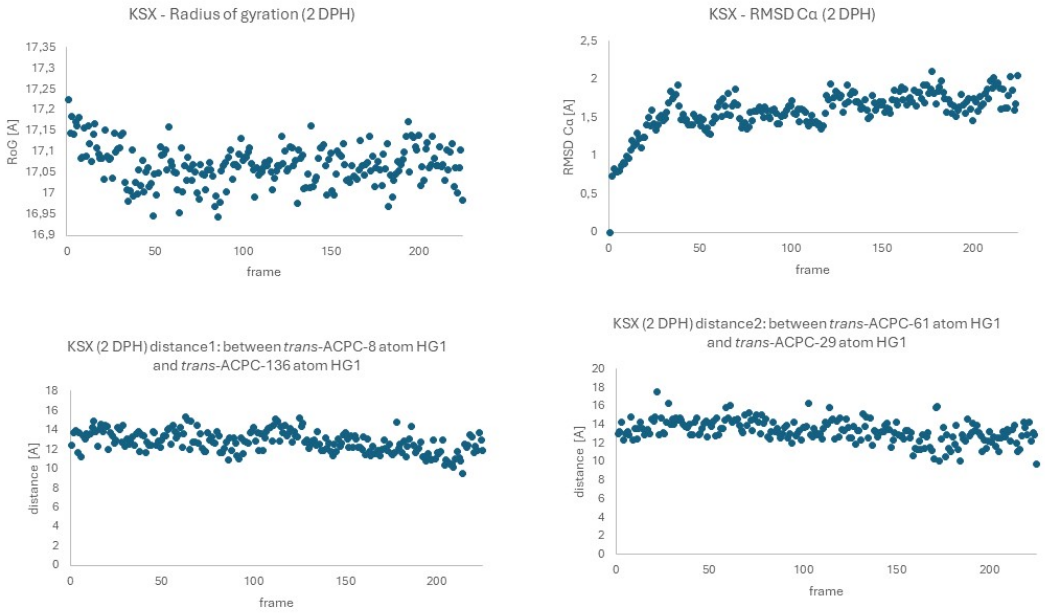

Figure St. The changes in the structure of **KSX** with alternative docking position of two DPH ligands over the course of a 24-ns molecular dynamics simulation. This includes variations in the radius of gyration, RMSD of the alpha carbon atom, as well as measurements of distance 1 (between a hydrogen atom of *trans*-ACPC residues 8 and 136) and distance 2 (between *trans*-ACPC residues 61 and 29). The selection of atoms for distance 1 and distance 2 serves as a means to monitor the dimensions of the channel at both ends.